

Good Artists Copy, Great Artists Steal: Model Extraction Attacks Against Image Translation Generative Adversarial Networks

Sebastian Szyller
contact@sebszyller.com
Aalto University
Helsinki, Finland

Tommi Gröndahl
tommi.grondahl@aalto.fi
Aalto University
Helsinki, Finland

Vasisht Duddu
vasisht.duddu@uwaterloo.ca
University of Waterloo
Waterloo, Canada

N. Asokan
asokan@acm.org
University of Waterloo
Waterloo, Canada

ABSTRACT

Machine learning models are typically made available to potential client users via inference APIs. *Model extraction attacks* occur when a malicious client uses information gleaned from queries to the inference API of a victim model F_V to build a *surrogate model* F_A that has comparable functionality. Recent research has shown successful model extraction attacks against image classification, and natural language processing models.

In this paper, we show the first model extraction attack against real-world generative adversarial network (GAN) *image translation models*. We present a framework for conducting model extraction attacks against image translation models, and show that the adversary can successfully extract functional surrogate models. The adversary is not required to know F_V 's architecture or any other information about it beyond its intended image translation task, and queries F_V 's inference interface using data drawn from the same domain as the training data for F_V .

We evaluate the effectiveness of our attacks using three different instances of two popular categories of image translation: (1) Selfie-to-Anime and (2) Monet-to-Photo (image style transfer), and (3) Super-Resolution (super resolution). Using standard performance metrics for GANs, we show that our attacks are effective in each of the three cases – the differences between F_V and F_A , compared to the target are in the following ranges: Selfie-to-Anime: Frechet Information Distance (FID) 13.36 – 68.66, Monet-to-Photo: FID 3.57 – 4.40, and Super-Resolution: Structural Similarity: 0.06 – 0.08 and Peak Signal-to-Noise Ratio: 1.43 – 4.46. Furthermore, we conducted a large scale (125 participants) user study on Selfie-to-Anime and Monet-to-Photo to show that human perception of the images produced by the victim and surrogate models can be considered equivalent, within an equivalence bound of Cohen's $d = 0.3$.

CCS CONCEPTS

• Security and privacy → Systems security; • Computing methodologies → Machine learning.

KEYWORDS

Generative Adversarial Network, Model stealing, Model extraction, Style transfer, Image translation

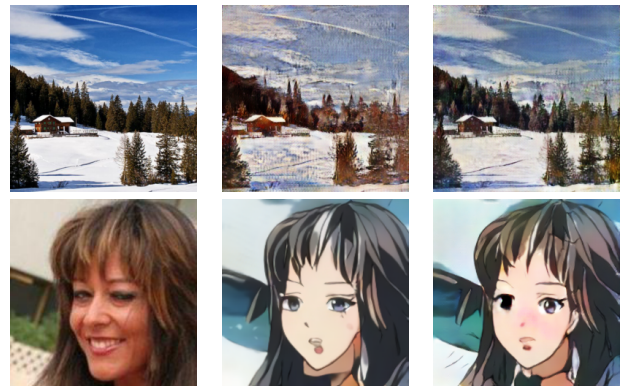


Figure 1: Example comparison of style transfer - left: original, center: V output, right: A output. Top row Monet-to-Photo style transfer, middle row Selfie-to-Anime style transfer. Images are down-scaled to fit the page.

1 INTRODUCTION

Machine learning models have become increasingly popular across a broad variety of application domains. They range from tasks like image classification and language understanding to those with strict safety requirements like autonomous driving or medical diagnosis. Machine learning is a multi-billion dollar industry [42] supported by technology giants, such as Microsoft, Google, and Facebook.

Recently *image translation* applications have become popular in social media. Examples include coloring old photos [18], applying cartoon based filters¹ or generating fake images of people (DeepFakes [43]). Features like face filters or face transformations are now an integral part of various popular applications such as TikTok, Snapchat or FaceApp. Such features are costly to create. They require data collection and sanitization, engineering expertise as well as computation resources to train *generative adversarial network* (GAN) models to implement these features. This represents a high barrier-to-entry for newcomers who want to offer similar features. Consequently, effective image translation models confer a business advantage on their owners.

¹<https://selfie2anime.com>

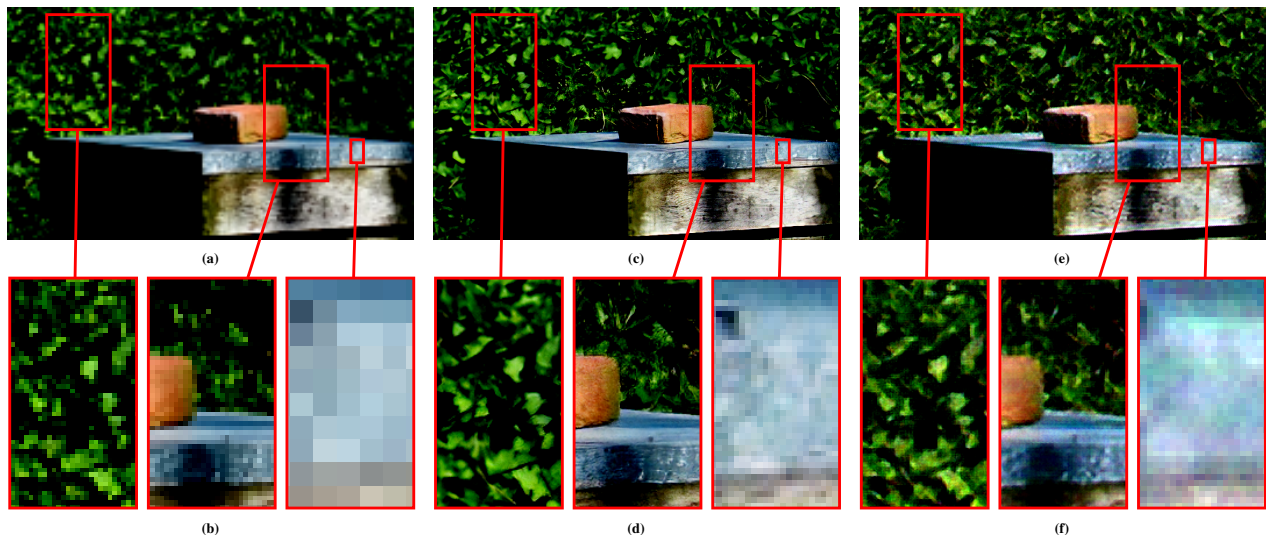


Figure 2: Example comparison of a Super-Resolution transformation. Left: original (a), center: \mathcal{V} output (c), right: \mathcal{A} output (e). Image up-scaled x4 from 175x100. We zoom in selected parts of the images (b,d,f) to show the difference in resolution among the three images.

Use of machine learning models is typically done in a *black-box* fashion – clients access the models via inference APIs, or the models are encapsulated within on-device sandboxed apps. However, a malicious client (adversary) can mount *model extraction attacks* [44] by querying a model and using the responses to train a local *surrogate model* that duplicates the functionality of the victim model. So far model extraction attacks have been shown to be successful in stealing image classifiers [9, 19, 21, 34, 37, 44], and natural language processing models [26, 45].

In this paper, we present the *first* model extraction attack targeting real-world *image translation* models. We show that an adversary can successfully build surrogate models mimicking the functionality of several types of image translation models (Figures 1-2). Our attack does not require the adversary to have access to victim’s training data, knowledge of victim model parameters or its architecture. We make the following contributions:

- (1) present the **first model extraction attack against image translation models** (Section 4), and
- (2) empirically demonstrate its effectiveness via
 - **quantitative analyses** using perceptual similarity metrics on three datasets spanning two types of image translation tasks: style transfer and image super resolution; the differences between the victim and surrogate models, compared to the target, are in the following ranges – Selfie-to-Anime: Frechet Information Distance (FID) 13.36 – 68.66, Monet-to-Photo²: FID 3.57 – 4.40, and Super-Resolution: Structural Similarity: 0.06 – 0.08 and Peak Signal-to-Noise Ratio: 1.43 – 4.46 (Section 5); and
 - an **extensive user study** ($n = 125$) on the style transfer tasks (Selfie-to-Anime and Monet-to-Photo) showing that

human perception of images produced by the victim and surrogate models are similar, within an equivalence bound of Cohen’s $d = 0.3$. (Section 5.4)

2 BACKGROUND AND RELATED WORK

In this section, we describe black-box model extraction attacks against machine learning systems in general, and some proposed defense approaches. Additionally, we give an overview of the use of generative adversarial networks (GANs) for image translation tasks, as well as a set of standardized metrics used to measure the effectiveness of such translations.

2.1 Model Extraction Attacks and Defenses

The goal of the adversary \mathcal{A} in model extraction attacks is to build a surrogate model to mimic the functionality of a victim model [34, 37]. The motivations for model extraction can be manifold: to use the surrogate model to offer a competing service [9, 34], or to probe the surrogate model to find adversarial examples that transfer to the victim model itself [21, 37]. \mathcal{A} conducts the attack by repeatedly querying the inference interface of the victim and using the responses to train the surrogate.

Model extraction techniques are similar to those used in active learning and knowledge distillation [3, 5, 29], except that model extraction happens in an adversarial setting. The techniques used for model extraction can differ depending on the assumptions regarding the knowledge and capabilities of the adversary. It is typical to assume that \mathcal{A} does not have access to the victim’s training data but may know the general domain (e.g., pictures of animals) [9, 37]. It is also customary to assume that \mathcal{A} does not know the exact architecture of the victim model, but may use known techniques to infer information about the victim architecture [4, 11, 16, 33, 46].

²The task is translating from photos to Monet paintings, but we refer to it as “Monet-to-Photo” to be consistent with the name of the dataset [51].

Previous work on model extraction attacks focuses primarily on image classification tasks. Initial work [21, 37, 44] focused on extracting exact replicas of simple classification models. \mathcal{A} would then use the surrogate model to craft adversarial examples more effectively [21, 37]. Subsequent work introduced attacks against ImageNet-scale models where \mathcal{A} 's goal was *functionality stealing* [9, 19, 34]. Other than image classification, there is a large body of work targeting other types of models - NLP models [26, 45], GNNs [13], and RNNs [41].

Existing model extraction defenses either attempt to identify \mathcal{A} by studying the query distribution [2, 21] or try to identify queries, like those that are close to decision boundaries [38, 49] or those that explore an abnormally large part of the hyperspace [24]. Alternatively, the defender can perturb the prediction vector before sending it back to the client in order to slow down the construction of effective surrogate models [22, 35].

Instead of detecting or defending against model extraction attacks, the defender can watermark their model and try to claim ownership if \mathcal{A} makes their surrogate model public. Watermarks can be embedded into the model during training by modifying its loss function [20] that makes it more likely that the watermarks transfer to the surrogate model. Alternately, model responses can be modified at the API level to embed a client-specific watermark into \mathcal{A} 's training data [40]. While there do exist watermarking schemes for GANs, they either assume the black-box generator style of GAN [47] or that \mathcal{A} is going to use specific data to launch the attack [48].

2.2 Generative Adversarial Networks

Generative Adversarial Networks (GANs) are a class of generative models which learn the underlying data distribution as a game between two models with conflicting objectives: a generator model G which generates new images from input noise and a discriminator model D which attempts to distinguish real images from the training data and fake images from G [12]. This is modeled as a minimax optimization problem: $\min_{\phi} \max_D V(G, D)$, where D maximises its gain $V(D, G)$ obtained by correctly distinguishing real and fake generated images. G minimizes the maximum gain by D and iteratively improves the quality of images to be close to the original training data points while fooling D . The overall optimization objective can be formulated as follows:

$$V(G, D) = \mathbb{E}_{x \sim p_{data}(x)} [\log(D(x))] + \mathbb{E}_{z \sim p_z(z)} [1 - \log(D(G(z)))] \quad (1)$$

where p_{data} is the distribution of the training data and p_z is the distribution learnt by G . This optimization is solved by alternatively training D and G using some variant of gradient descent, e.g. SGD or Adam. The outstanding performance of GANs have resulted in their widespread adoption for different applications addressing several image processing and image translation tasks. In this work, we consider two main applications of image to image translations: style transfer [18, 25, 51] and image super resolution [28].

Style Transfer. GANs have been used to translate images from one style to another. [18]. Prior work explored several image style transfer tasks such as changing seasons, day to night, black and white to colored, and aerial street images to maps [18, 25, 51]. Some specific

tasks have been extensively adopted as filters in social networks such as Instagram, Snapchat and FaceApp, e.g. changing human faces to anime characters [25], aging, hair coloring or swapping genders [6, 23]. These are trained using GANs. Style transfer GANs can be trained using paired image-to-image data with a Pix2Pix model [18] in a supervised fashion - each unstyled image has its styled counterpart. However, for many complex tasks, such supervised image to image translation training data is difficult, if not impossible, to obtain. To address this, training generative models using unpaired and uncorrelated mappings of the images in the input source domain to the target output domain has been proposed (e.g. CycleGAN, UGATIT [25, 51]).

Pix2Pix [18]. The Pix2Pix architecture uses a UNet Generator Model which downsamples an input image from the source domain and outputs an upsampled image in the target domain. This is similar to the encoder-decoder architecture seen in autoencoders. In addition, Pix2Pix uses a PatchGAN discriminator network which takes the input image from the source domain and the image from the target domain to determine whether the generated output image from the target domain is from the real distribution or from the UNet generator. To train a Pix2Pix model, the UNet generator is trained to minimize the loss of correctly translating the input source domain image to the target domain image (*IdentityLoss*) while additionally minimizing the adversarial loss that captures the success of discriminator, to produce realistic target domain images. The overall loss optimized includes: $GeneratorLoss = AdversarialLoss + \lambda * IdentityLoss$.

CycleGAN [51]. We describe the loss functions and optimizations used in a typical CycleGAN. Many other generative models are usually variations of this basic architecture. CycleGAN consists of two GANs, i.e. two generative models and two discriminators. One of the GANs maps images from the source domain to the target domain while the second GAN maps images from the target domain back to the source domain. Both generators are similar to generators in Pix2Pix and map images from one domain to the other by downsampling the image, followed by upsampling the image to the target domain. Like Pix2Pix, CycleGAN uses adversarial loss with respect to the discriminators to ensure that the generator outputs domain images close to real images, and Identity Loss to ensure similarity between the generated image and real target domain image. Additionally, CycleGAN uses the optimized cycle consistency loss. It ensures that an image when mapped from the source domain to the target domain and back to the source domain are as similar as possible.

UGATIT [25]. In addition to the architecture and optimization of the CycleGAN, UGATIT utilizes convolutional neural networks as an attention module to identify and extract major features in images. This allows for finer optimization while translating input images to the target domain.

Image Super Resolution. The task of mapping low resolution images to high resolution images is performed using a GAN architecture. The generator includes residual blocks that alleviate the vanishing gradient problem and hence, enable deeper models that give better results. The generator outputs a high resolution (HR) image that is an up-scaled version of its low resolution input counterpart. The discriminator differentiates between the generated HR image with the ground truth HR image. The generator parameters are updated similarly to the optimization in a generic GAN (Equation 1).

2.3 Metrics

We consider several metrics for comparing the quality of images generated by the victim and surrogate models. Unlike discriminative models such as image classifiers that rely on accuracy with respect to ground truth, we need to be able to objectively compare the performance of the victim and surrogate models without necessarily having access to any ground truth. The metrics we discuss below serve this purpose.

Structural Similarity (SSIM) [50]. For two image windows x and y of same size $N \times N$, SSIM is computed as follows:

$$SSIM(x, y) = \frac{(2\mu_x\mu_y + c_1)(2\sigma_{xy} + c_2)}{(\mu_x^2 + \mu_y^2 + c_1)(\sigma_x^2 + \sigma_y^2 + c_2)} \quad (2)$$

where μ is the mean of pixels over the windows, σ^2 is the variance of pixel values and σ_{xy} is the covariance, c_1 and c_2 are constants to ensure numerical stability. SSIM computes the perceived image quality and compares two images with one of the images as a reference. Dissimilar images are scored as 0.0 while the same images are given a score of 1.0.

Peak Signal to Noise Ratio (PSNR) [15]. PSNR is the ratio of the signal (image content) and the noise that lowers the fidelity of the image:

$$PSNR = 20 \cdot \log_{10} \frac{MAX}{\sqrt{MSE}} \quad (3)$$

where MAX is maximum range of pixel value in the image given by $2^b - 1$ where b is the number of bits. MSE is the mean squared error which is the squared difference between the image pixel values and the mean value.

We use SSIM and PSNR to estimate and compare the quality of the generated super resolution image to the original HR ground truth image. For the style transfer tasks, we consider Frechet Inception Distance typically used to evaluate GANs.

Frechet Inception Distance (FID). FID measures the distance between the features of real and generated images and is used to estimate the quality of images from GANs [14, 31]. FID uses the output features from the last pooling layer before the output prediction layer from the Inceptionv3 network. The distance between the feature distributions for two sets of images is computed using Wasserstein (Frechet) distance. Low scores correspond to higher quality generated images but the magnitude of what constitutes high or low FID depends on the domain and complexity of measured images.

We also experimented with using pixel-based metrics [39] but decided to use FID because it appeared to match up more closely with human perception. In general, the problem of defining accurate metrics that represent human perception of images is still an open problem.

3 PROBLEM STATEMENT

3.1 Adversary Model

The adversary \mathcal{A} wants to build a surrogate model $F_{\mathcal{A}}$ to mimic the functionality of a model $F_{\mathcal{V}}$ belonging to the victim \mathcal{V} . \mathcal{A} is aware of the purpose of $F_{\mathcal{V}}$, e.g. style transfer from Monet paintings, and can choose an appropriate model architecture of $F_{\mathcal{A}}$. However, \mathcal{A} is not aware of the exact architecture of $F_{\mathcal{V}}$. \mathcal{A} conducts the attack

with any data $X_{\mathcal{A}}$ they want but they have no knowledge of the exact training data \mathcal{V} used. Crucially, we assume that \mathcal{A} does not have access to any *source style* images S . We assume that \mathcal{V} wants to keep S secret because it is valuable and difficult to obtain. \mathcal{A} has only *black-box* access to $F_{\mathcal{V}}$. \mathcal{A} uses $X_{\mathcal{A}}$ and $X_{\mathcal{A}_S} = F_{\mathcal{V}}(X_{\mathcal{A}})$ to train $F_{\mathcal{A}}$ in any way they want. \mathcal{A} 's goal is to duplicate the *functionality* of $F_{\mathcal{V}}$ as closely as possible.

3.2 Goals

\mathcal{A} 's goal is not to optimize the style transfer task itself but rather to achieve a level of performance comparable to $F_{\mathcal{V}}$. Therefore, they use $F_{\mathcal{V}}$ as an oracle to obtain its "ground truth" for training $F_{\mathcal{A}}$. \mathcal{A} wants to either keep using the service without paying or to offer a competitive service at a discounted price. \mathcal{A} is not trying to obtain the exact replica of $F_{\mathcal{V}}$. Upon a successful model extraction attack, images styled by $F_{\mathcal{A}}$ should be comparable to those produced by $F_{\mathcal{V}}$. Assuming $F_{\mathcal{V}}$ is a high quality style-transfer model, then the attack is considered successful if $F_{\mathcal{V}}(X) \approx F_{\mathcal{A}}(X)$.

4 EXTRACTING IMAGE TRANSLATION MODELS

In this section, we describe how to launch model extraction attacks against image translation models.

4.1 System Components

We target two most popular applications of GANs for image translation: image style transfer (Selfie-to-Anime and Monet-to-Photo) and image super resolution. The attack setting considers \mathcal{V} 's model $F_{\mathcal{V}}: X \rightarrow X_S$ that maps an unstyled original image X to the corresponding styled image X_S . The style template S is added to the input image. \mathcal{A} aims to steal the styling functionality of $F_{\mathcal{V}}$ that maps the input image to the corresponding styled image without explicit access to the secret styling template S .

4.2 Attack Methodology.

\mathcal{A} queries $F_{\mathcal{V}}$ using \mathcal{V} 's API to obtain the corresponding styled $X_{\mathcal{A}_S}$ images generated by $F_{\mathcal{V}}$. This is consistent with the practical settings likely to be encountered in real world applications. This pair of unstyled input and styled output image ($X_{\mathcal{A}}, X_{\mathcal{A}_S}$) constitutes the surrogate training data used by \mathcal{A} to train the surrogate model $F_{\mathcal{A}}$. Since \mathcal{A} relies on training $F_{\mathcal{A}}$ using pairs of data points, we use paired image translation GANs as our attack model. As previously explained, training paired translation models is not realistic in many real world applications due to the lack of styled images. However in our case, \mathcal{A} leverages the fact that they can obtain as many X_S by querying $F_{\mathcal{V}}$. Additionally, our attack makes no assumptions regarding the styling technique used to generate the styled images. However, models that we target do require GANs for high quality transformations. Even though the styling template S applied to unstyled input images by $F_{\mathcal{V}}$ is learned explicitly from images, it can be stolen and implicitly embedded in $F_{\mathcal{A}}$.

More formally, from the set of possible mappings \mathcal{F} , the mapping $F_{\mathcal{V}}: X \rightarrow X_S$ is optimal if according to some quantitative criterion \mathcal{M}_S , the resulting transformation captures the style S by maximizing

$\mathcal{M}_S(X_S, S)$:

$$F_{\mathcal{V}} = \arg \max_{F'_{\mathcal{V}} \in \mathcal{F}} \mathcal{M}_S(X_S, S) \quad (4)$$

as well as retains the semantics of the input image $\mathcal{M}_X(X, X_S)$ by maximizing another criterion \mathcal{M}_X :

$$F_{\mathcal{V}} = \arg \max_{F'_{\mathcal{V}} \in \mathcal{F}} \mathcal{M}_X(X, X_S) \quad (5)$$

\mathcal{A} 's goal is to learn the same kind of mapping $F_{\mathcal{A}} : X_{\mathcal{A}} \rightarrow X_{\mathcal{A}_S}$ using images obtained from $F_{\mathcal{V}}$. This transformation must be successful according to both criteria $\mathcal{M}_X(X_{\mathcal{A}}, X_{\mathcal{A}_S})$ and $\mathcal{M}_S(X_{\mathcal{A}_S}, S)$:

$$\begin{aligned} F_{\mathcal{A}} &= \arg \max_{F'_{\mathcal{A}} \in \mathcal{F}} \mathcal{M}_X(X_{\mathcal{A}}, X_{\mathcal{A}_S}) \quad \text{and} \\ F_{\mathcal{A}} &= \arg \max_{F'_{\mathcal{A}} \in \mathcal{F}} \mathcal{M}_S(X_{\mathcal{A}_S}, S) \end{aligned} \quad (6)$$

However, \mathcal{A} does not have access to S . Instead, they use a proxy metric $\mathcal{M}_{\mathcal{P}}(F_{\mathcal{V}}, F_{\mathcal{A}}, X)$. Abusing notation, we define it as:

$$\begin{aligned} F_{\mathcal{A}} &= \arg \max_{F'_{\mathcal{A}} \in \mathcal{F}} \mathcal{M}_{\mathcal{P}}(F_{\mathcal{V}}, F_{\mathcal{A}}, X) \quad \text{s.t.} \\ &\text{if } F_{\mathcal{A}}(X) \approx F_{\mathcal{V}}(X) \quad \text{then} \\ F_{\mathcal{A}} &= \arg \max_{F'_{\mathcal{A}} \in \mathcal{F}} \mathcal{M}_X(X_{\mathcal{A}}, X_{\mathcal{A}_S}) \quad \text{and} \\ F_{\mathcal{A}} &= \arg \max_{F'_{\mathcal{A}} \in \mathcal{F}} \mathcal{M}_S(X_{\mathcal{A}_S}, S) \end{aligned} \quad (7)$$

In other words, we assume that if images produced by $F_{\mathcal{A}}$ are similar to those produced by $F_{\mathcal{V}}$, then $F_{\mathcal{A}}$ has successfully learned the style S .

We apply our attacks to the following three settings.

Setting 1: Monet-to-Photo. Monet-to-Photo is a style transfer task in which a picture of a scene is transformed to look as if it was painted in Claude Monet's signature style. We train $F_{\mathcal{V}}$ as an unpaired image to image translation problem, i.e, the training data consists of unordered and uncorrelated photos of landscapes which are styled according to the images in the styling template S which are Monet paintings. S is secret and not visible to \mathcal{A} . The model learns the features in Monet paintings and applies them to translate generic photos. \mathcal{A} queries $F_{\mathcal{V}}$ with images $X_{\mathcal{A}}$ from a different dataset than \mathcal{V} 's training data and obtains corresponding $X_{\mathcal{A}_S} = F_{\mathcal{V}}(X_{\mathcal{A}})$. $F_{\mathcal{A}}$ is trained using this generated dataset $(X_{\mathcal{A}}, X_{\mathcal{A}_S})$ as a paired image to image translation problem between the two domains.

Setting 2: Selfie-to-Anime. Selfie-to-Anime is used as part of a real world web application which allows users to upload their selfie and convert it to a corresponding anime image³. We do not attack the actual web interface due to its terms of service on reverse engineering and scraping. However, the authors disclose the data and architecture [25] used to train their model, and we use it to train our $F_{\mathcal{V}}$. The training data is unpaired - it consists of a training set of selfie images, and a styling template S consisting of anime images. \mathcal{A} queries $F_{\mathcal{V}}$ with images $X_{\mathcal{A}}$ from a different dataset than \mathcal{V} 's training data and obtains corresponding $X_{\mathcal{A}_S} = F_{\mathcal{V}}(X_{\mathcal{A}})$. $F_{\mathcal{A}}$ is trained using this generated dataset $(X_{\mathcal{A}}, X_{\mathcal{A}_S})$ as a paired image to image translation problem between the two domains.

³<https://selfie2anime.com/>

Table 1: Summary of datasets used to for training $F_{\mathcal{V}}$ and $F_{\mathcal{A}}$.

Task	\mathcal{V} Data	\mathcal{A} Data	Benchmark Data
Monet to Photo	Monet2Photo	Intel	Landscape
	Train	Test	Test
	6287	751	4319
Selfie to Anime	Selfie2Anime	CelebA	LFW
	Train	Test	Test
	3400	100	13233
Super Resolution	DIV2K	FLICKR2K	SRBenchmark
	Train	Test	Test
	800	200	294

Setting 3: Super-Resolution. In Super-Resolution a low resolution image is upscaled to its high resolution counterpart using a GAN. We consider mapping low resolution images, (using a 4x bicubic downscaling) to their high resolution counterparts with 4x upscaling. $F_{\mathcal{V}}$'s generator is trained in a supervised fashion using a paired dataset (X_{lr}, X_{hr}) of low resolution and corresponding high resolution images. Here X_{hr} corresponds to X_S . There is no explicit styling template S . \mathcal{A} queries $F_{\mathcal{V}}$ with publicly available low resolution images $X_{\mathcal{A}_{lr}}$ to obtain the corresponding high resolution image $X_{\mathcal{A}_{hr}} = F_{\mathcal{V}}(X_{\mathcal{A}_{lr}})$. This paired surrogate data $(X_{\mathcal{A}_{lr}}, X_{\mathcal{A}_{hr}})$ is used to train $F_{\mathcal{A}}$.

5 EVALUATION

5.1 Datasets

Monet-to-Photo. $F_{\mathcal{V}}$ is trained using the Monet2Photo [36] dataset consisting of 1193 Monet paintings and 7038 natural photos divided into train and test sets. For training $F_{\mathcal{A}}$, we use the Intel Image Classification dataset [7]. It consists of 14,034 of images of various nature and city landscapes. As the benchmark dataset, we choose the Landscape [32] dataset that contains 13,233 images from the same domain but was not used to train either model.

Selfie-to-Anime. $F_{\mathcal{V}}$ is trained on the selfie2anime dataset [10] which comprises 3400 selfies and 3400 anime faces as part of the training data, and 100 selfies and 100 anime faces in the test set. \mathcal{A} uses the CelebA [30] dataset for attacking \mathcal{V} which consists of 162,770 photos of celebrities. For the benchmark dataset, we use the LFW dataset [17] which contains a test set of 13233 selfie images.

Super-Resolution. $F_{\mathcal{V}}$ is trained using the DIV2K [1] dataset that consists of 800 pairs of low resolution and corresponding high resolution images in the training set, and 200 image pairs for validation and testing. \mathcal{A} uses the FLICKR2K dataset for the extraction. It consists of 2650 train (and 294 test images). We create the SRBeckmark dataset by combining multiple benchmarking datasets used for super resolution model evaluations including SET5 [27], SET14 [27], URBAN100 [27] and BSD100 [27] containing 294 images. All high resolution images are 4x bicubic downsampled.

5.2 Architectures

Monet to Photo. We use the state of the art CycleGAN [51] architecture as the $F_{\mathcal{V}}$ architecture. For $F_{\mathcal{A}}$ architecture we use a paired image-to-image translation model Pix2Pix [18].



Figure 3: Example of successful transformations produced by $F_{\mathcal{V}}$ and $F_{\mathcal{A}}$ that are visually similar.

Selfie to Anime. We use the UGATIT generative model [25] as the $F_{\mathcal{V}}$ architecture which is similar to CycleGAN with an additional attention module to identify and optimize important features. This is the model used by the Selfie2Anime service⁴. Like for Monet-to-Photo, we use a paired image-to-image translation model Pix2Pix [18] for $F_{\mathcal{A}}$.

Super Resolution. For the $F_{\mathcal{V}}$ architecture we use the state of the art SRGAN model [28] while for $F_{\mathcal{A}}$ we use a similar SRResNet model [28] with ResNet convolutional units.

5.3 Experiments

Tables 2 to 4 summarize the results of our experiments. We report the mean value for a given distance metric. We also report standard deviations where applicable. In Tables 2 and 3 we report the effectiveness of the attack measured using the FID score for style transfer settings. In Table 4 we report the effectiveness of the attack measured using PSNR and SSIM for the Super-Resolution setting. In each setting for each dataset, we report on three different experiments:

- (A) **effectiveness of $F_{\mathcal{V}}$ transformations:** this is the baseline performance of $F_{\mathcal{V}}$ with respect to the original test set (cell (A) in Tables 2 to 4).
- (B) **comparison of $F_{\mathcal{A}}$ and $F_{\mathcal{V}}$:** this is measured using the proxy metric (Equation 7) that \mathcal{A} uses to assess the effectiveness of $F_{\mathcal{A}}$ in terms of how closely its outputs resemble the outputs of $F_{\mathcal{V}}$ (cell (B) in Tables 2 to 4).
- (C) **effectiveness of $F_{\mathcal{A}}$ transformations:** this is measured the same way as (A). Note that \mathcal{A} cannot directly compute this effectiveness metric because they do not have access to the ground truth (in the form of the styling set S or paired images in the case of Super-Resolution; cell (C) in Tables 2 to 4).

For Monet-to-Photo, we can see that our attack is effective at extracting $F_{\mathcal{V}}$. In Table 2, we report the FID scores for the three experiments using two test sets. In all cases, we see that $F_{\mathcal{A}}$ performs comparably to $F_{\mathcal{V}}$.

Our attack is effective at extracting a Selfie-to-Anime $F_{\mathcal{V}}$. In Table 3, we report the FID scores for the three experiments, using two test sets. We observe a large FID score for the \mathcal{V} 's test set (Selfie2Anime). However, using a benchmark test set (LFW), we observe that both models compare similarly and produce similar styled images, c.f. Figure 3. Additionally, we observe that many transformations are qualitatively similar (both models successfully produce anime faces) even though the resulting transformations are different, c.f. Figure 4.

⁴<https://selfie2anime.com/>



Figure 4: $F_{\mathcal{V}}$ and $F_{\mathcal{A}}$ learn different representations and can produce transformations that have different features even though both transformations are comparable in their effectiveness.

Table 2: FID of victim and attacker models for Monet-to-Photo.

Output Distribution	Test Set	Compared Distribution	
		\mathcal{V} Output	Monet Paintings
\mathcal{V} Output	Monet2Phto Test	N/A	(A) 58.05
	Landscape	N/A	(A) 49.59
\mathcal{A} Output	Monet2Phto Test	(B) 42.86	(C) 61.62
	Landscape	15.38	(C) 53.99

Table 3: FID of victim and attacker models for Selfie-to-Anime.

Output Distribution	Test Set	Compared Distribution	
		\mathcal{V} Output	Anime Faces
\mathcal{V} Output	Selfie2Anime	N/A	(A) 69.02
	LFW Test	N/A	(A) 56.06
\mathcal{A} Output	Selfie2Anime	(B) 138.61	(C) 137.68
	LFW Test	19.67	(C) 69.42

Table 4: PSRN and SSIM of victim and attacker models for Super-Resolution. We report the mean value and standard deviation computed for two test sets.

(a) **SSIM. Comparing $F_{\mathcal{A}}$ to $F_{\mathcal{V}}$ captures the true performance.**

Output Distribution	Test Set	Compared Distribution	
		\mathcal{V} Output	Original high-res
\mathcal{V} Output	DIV2K Test	N/A	(A) 0.74 ± 0.10
	SRBENCHMARK	N/A	(A) 0.69 ± 0.23
\mathcal{A} Output	DIV2K Test	(B) 0.75 ± 0.16	(C) 0.80 ± 0.20
	SRBENCHMARK	0.76 ± 0.18	(C) 0.61 ± 0.23

(b) **PSNR. Comparing $F_{\mathcal{A}}$ to $F_{\mathcal{V}}$ captures the true performance.**

Output Distribution	Test Set	Compared Distribution	
		\mathcal{V} Output	Original high-res
\mathcal{V} Output	DIV2K Test	N/A	(A) 24.67 ± 3.63
	SRBENCHMARK	N/A	(A) 22.59 ± 9.51
\mathcal{A} Output	DIV2K Test	(B) 24.74 ± 9.21	(C) 23.24 ± 7.17
	SRBENCHMARK	20.64 ± 7.33	(C) 18.13 ± 6.73

Finally, our attack is effective at extracting the Super-Resolution $F_{\mathcal{V}}$, c.f. Table 4. Both in the case of SSIM (Table 4a) and PSNR (Table 4b), $F_{\mathcal{A}}$ performs similarly to $F_{\mathcal{V}}$. This holds for the proxy comparison between $F_{\mathcal{V}}$ and $F_{\mathcal{A}}$, as well as w.r.t. the original high resolution images. The differences in mean values are within the corresponding standard deviation ranges.

5.4 User Study

Since distance metrics do not necessarily capture human perception, we conducted an extensive user study to evaluate how humans rate the image translation tasks.

Materials. We designed a questionnaire in Google Forms which we shared with the participants (see supplementary materials).

Participants. We conducted the user study with 125 participants invited through social media (Twitter, LinkedIn, Facebook), institutional channels (Slack, Teams, Telegram groups) and personal communication. We collected basic demographics about the participants, including age, highest obtained education, and gender. Our user study data collection conforms to our institution’s data management guidelines. No personally identifiable information was collected as part of the study. Figure 5 represents the distribution of demographics of the participants.

Design of User Study. In the questionnaire, we first introduced the problem of image style transfer with examples of Monet paintings and anime images. We also included an explanation that the study aims to evaluate which of the shown style transformations are successful in the participant’s personal opinion, and does not evaluate their skill in making this judgement. Participants then evaluated the style transformations using a Likert scale from 1 to 5. A score of 5 indicated that the result looked very similar to a Monet painting of the input scene or an anime character corresponding to the source selfie photo, and a score of 1 that there was no such resemblance. The website and the questionnaire are available as a supplement.⁵

Procedure. We conducted the user study on two style transfer settings. For both tasks, we included 20 image pairs formed by an original unstyled image and its corresponding styled variant. Half of the pictures (10) were styled with $F_{\mathcal{V}}$ and the other half with $F_{\mathcal{A}}$.

Results. Figures 6 and 7 show the distribution of scores for $F_{\mathcal{V}}$ and $F_{\mathcal{A}}$ in the Monet-to-Photo and Selfie-to-Anime test settings, respectively. Our evaluation concerns whether the differences between results obtained from $F_{\mathcal{V}}$ and $F_{\mathcal{A}}$ were *statistically significant*. We first conducted a *t-test*, which yields a conditional probability (*p-value*) for receiving values deviating equally or more between the sample statistics as observed in the experiments, under the *null hypothesis* of equal underlying population distributions. The outcome is considered statistically significant if *p* exceeds the *significance threshold* α , which we set to 0.05. Since sample variances were unequal between $F_{\mathcal{V}}$ and $F_{\mathcal{A}}$, we used Welch’s t-test instead of Student’s t-test.

The null hypothesis of equivalent population distributions was rejected for Monet-to-Photo ($F_{\mathcal{V}}$ ’s score mean = 3.20 and std = 1.59; $F_{\mathcal{A}}$ ’s score mean = 2.91 and std = 1.76; $p = 1.8e - 8$) but not for Selfie-to-Anime ($F_{\mathcal{V}}$ ’s score mean = 3.11 and std = 1.76; $F_{\mathcal{A}}$ ’s score mean = 3.08 and std = 1.50; $p = 0.63$). In other words, the probability of obtaining results deviating between $F_{\mathcal{V}}$ and $F_{\mathcal{A}}$ as much as observed (or more) would be very high for Selfie-to-Anime but very low for Monet-to-Photo, if $F_{\mathcal{V}}$ and $F_{\mathcal{A}}$ indeed performed similarly.

However, the t-test alone is insufficient to evaluate the divergence between $F_{\mathcal{V}}$ and $F_{\mathcal{A}}$. We additionally performed a *two one-sided t-test* (TOST) for *equivalence* to test whether the results fall between *equivalence bounds*. As the bounds, we chose the range $[-0.3, 0.3]$

for *Cohen’s d*, which is the mean difference between the models’ scores standardized by their pooled standard deviations [8]. The null hypothesis is reversed from the standard t-test, now assuming the *non-equivalence* between underlying population distributions. The null hypothesis is rejected if the observed difference falls within the equivalence bounds.

For Selfie-to-Anime the null hypothesis was rejected within the equivalence bounds of $[-0.11, 0 - 11]$ ($p = 0.0476$), and for Monet-to-Photo within $[-0.38, 0, 38]$ ($p = 0.04829$), using $\alpha = 0.05$. Both fall within $[-0.3, 0.3]$ for Cohen’s *d*, which corresponds to the raw value range of approximately $[-0.50, 0.50]$ in Selfie-to-Anime and $[-0.49, 0.49]$ in Monet-to-Photo. Hence, we reject the non-equivalence of $F_{\mathcal{V}}$ and $F_{\mathcal{A}}$ in **both** test settings.

Hence, while a statistically significant difference between $F_{\mathcal{V}}$ and $F_{\mathcal{A}}$ was observed in Monet-to-Photo, it was too small to count as sufficiently large for meaningful non-equivalence in TOST. In Selfie-to-Anime, both the t-test and TOST supported rejecting the non-equivalence of $F_{\mathcal{V}}$ and $F_{\mathcal{A}}$. We therefore conclude that $F_{\mathcal{A}}$ successfully achieved **performance close to $F_{\mathcal{V}}$ based on human judgement**.

5.5 Discussion

Metrics. In the Super-Resolution setting, we have access to ground truth images in the form of original high resolution photos. Therefore, the metrics we used for Super-Resolution (PSNR and SSIM) are sufficient for making firm conclusions about the comparative effectiveness of $F_{\mathcal{V}}$ and $F_{\mathcal{A}}$. This is why a separate user study for Super-Resolution was unnecessary.

For the style transfer settings (Monet-to-Photo and Selfie-to-Anime) there is no such ground truth – given an input image, there is no quantitative means of assessing whether the corresponding output image looks like a Monet painting or an anime figure. Our experience with pixel-based metrics (Section 2.3) underscored the possibility that perceptual similarity metrics may not be adequate. This is our motivation for a separate user study to assess the effectiveness in the Monet-to-Photo and Selfie-to-Anime settings. The distance metric we used (FID) indicated that the output distributions of $F_{\mathcal{V}}$ and $F_{\mathcal{A}}$ are close, as did manual inspection of a random subset of the transformations. The user study also confirmed that both models are similar within reasonable equivalence bounds. However, the user study indicated that $F_{\mathcal{V}}$ and $F_{\mathcal{A}}$ are more similar in the Selfie-to-Anime setting than in the Monet-to-Photo setting (Figures 6 and 7) whereas the FID metric indicated otherwise (Tables 2 and 3). This highlights the importance of more robust quantitative metrics for comparing human perception of image similarity.

Defenses. In this work, we emphasize the feasibility of launching the attack against realistic $F_{\mathcal{V}}$, and show that having obtained $F_{\mathcal{A}}$, \mathcal{A} can launch a competing service. The next step would be to explore ways of protecting against such attacks. None of the existing defenses against model extraction attacks explained in Section 2 apply to image translation models. Most of these defenses [2, 21, 24, 38, 49] rely on examining the distribution of queries from clients to differentiate between queries from legitimate clients and queries from model extraction adversaries. In our adversary model, we assumed that \mathcal{A} uses natural images drawn from the same domain as \mathcal{V} . As a result, none of those defenses are applicable to our attack. Other

⁵All study materials and results will be made public upon publication of this work.

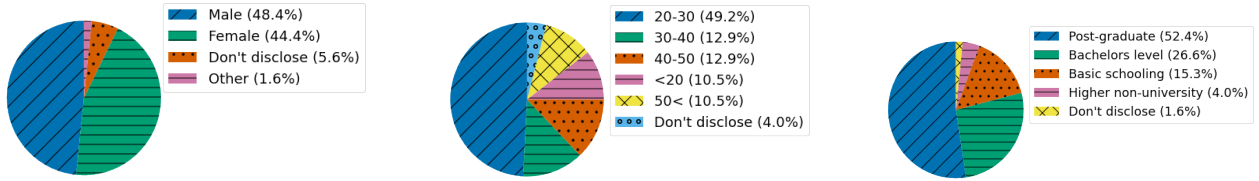


Figure 5: Distribution of participant demographics. Left to right: gender, age and highest-completed education.

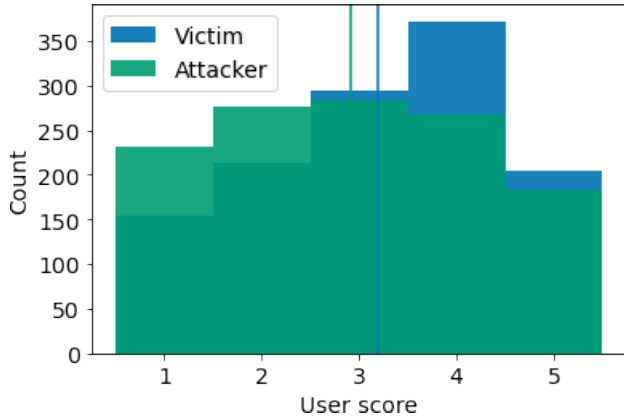


Figure 6: Monet-to-Photo. Comparison of scores assigned by the user study participants. For F_V score mean = 3.20 and std = 1.59, and for F_A mean = 2.91 and std = 1.76. Vertical lines indicate means of corresponding distributions.

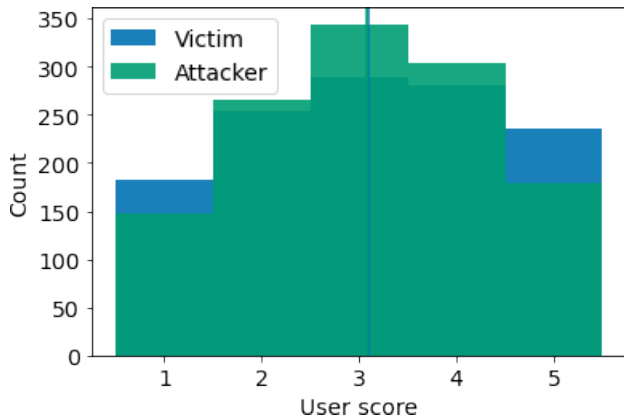


Figure 7: Selfie-to-Anime. Comparison of scores assigned by the user study participants. For F_V score mean = 3.11 and std = 1.76, and for F_A mean = 3.08 and std = 1.50. Vertical lines indicate means of corresponding distributions.

defenses [22, 35] rely on perturbing prediction vectors which is only applicable to attacks against classifiers.

Alternatively, \mathcal{V} could attempt to embed a watermark into the model such that all output images contain a trigger that would transfer to F_A . This would allow \mathcal{V} to prove ownership and thus, deter \mathcal{A} that wants to launch a competing service but it does not stop the attack on its own. However, as in the case of detection techniques discussed above, existing watermarking schemes intended for classifiers are not suitable for black-box extraction of image translation models.

One way, to prevent \mathcal{A} from extracting the model, would be to investigate ways of extending adversarial examples and data poisoning to image translation models, and incorporate them as a defense mechanism. \mathcal{V} could add imperceptible noise to the output images, designed to make the training of F_A impossible or at least slow it down such that it is not economically viable. We leave the exploration of such defenses as future work.

6 CONCLUSION

We showed that model extraction of real-world image translation models is a practical, and hence realistic, threat. Although there are some proposed defenses against model extraction attacks against image classifiers, they do not apply to image translation. Developing effective defenses against extraction of image translation models is thus an urgent open problem.

Our evaluation also underscores the fact that standard quantitative metrics for perceptual similarity of images (FID or pixel-based metrics), do not necessarily represent how humans perceive image similarity.

REFERENCES

- [1] Eirikur Agustsson and Radu Timofte. 2017. NTIRE 2017 Challenge on Single Image Super-Resolution: Dataset and Study. In *The IEEE Conference on Computer Vision and Pattern Recognition (CVPR) Workshops*.
- [2] Buse Gul Atli, Sebastian Szyller, Mika Juuti, Samuel Marchal, and N. Asokan. 2020. Extraction of Complex DNN Models: Real Threat or Boogeyman?. In *Engineering Dependable and Secure Machine Learning Systems*. 42–57.
- [3] Antonio Barbalau, Adrian Cosma, Radu Tudor Ionescu, and Marius Popescu. 2020. Black-Box Ripper: Copying black-box models using generative evolutionary algorithms. In *NeurIPS*.
- [4] Lejla Batina, Shivam Bhasin, Dirmanto Jap, and Stjepan Picek. 2019. CSI NN: Reverse Engineering of Neural Network Architectures Through Electromagnetic Side Channel. In *28th USENIX Security Symposium (USENIX Security 19)*.
- [5] Varun Chandrasekaran, Kamalika Chaudhuri, Irene Giacomelli, Somesh Jha, and Songbai Yan. 2020. Exploring Connections Between Active Learning and Model Extraction. In *29th USENIX Security Symposium (USENIX Security 20)*.
- [6] Yunjey Choi, Minje Choi, Munyoung Kim, Jung-Woo Ha, Sunghun Kim, and Jaegul Choo. 2018. StarGAN: Unified Generative Adversarial Networks for Multi-Domain Image-to-Image Translation. In *Proceedings of the IEEE Conference on Computer Vision and Pattern Recognition (CVPR)*.
- [7] Intel Image Scene Classification. Accessed on April 12 2021. <https://kaggle.com/puneet6060/intel-image-classification>
- [8] Jacob Cohen. 1988. *Statistical Power Analysis for the Behavioral Sciences*. Routledge, New York.

- [9] Jacson Rodrigues Correia-Silva, Rodrigo F Berriel, Claudine Badue, Alberto F de Souza, and Thiago Oliveira-Santos. 2018. Copycat CNN: Stealing Knowledge by Persuading Confession with Random Non-Labeled Data. In *2018 International Joint Conference on Neural Networks (IJCNN)*. IEEE, 1–8.
- [10] Picture datasets of selfie2anime. Accessed on April 12 2021. <https://kaggle.com/arnaud58/selfie2anime>
- [11] Vasisht Duddu, Debasis Samanta, D Vijay Rao, and Valentina E. Balas. 2019. Stealing Neural Networks via Timing Side Channels. In *arXiv 1812.11720*.
- [12] Ian J. Goodfellow, Jean Pouget-Abadie, Mehdi Mirza, Bing Xu, David Warde-Farley, Sherjil Ozair, Aaron Courville, and Yoshua Bengio. 2014. Generative Adversarial Nets. In *Proceedings of the 27th International Conference on Neural Information Processing Systems*. 2672–2680.
- [13] Xinlei He, Jinyuan Jia, Michael Backes, Neil Zhenqiang Gong, and Yang Zhang. 2020. Stealing Links from Graph Neural Networks. *arXiv:cs.CR/2005.02131*
- [14] Martin Heusel, Hubert Ramsauer, Thomas Unterthiner, Bernhard Nessler, and Sepp Hochreiter. 2017. GANs Trained by a Two Time-Scale Update Rule Converge to a Local Nash Equilibrium. In *Proceedings of the 31st International Conference on Neural Information Processing Systems*.
- [15] A. Horé and D. Ziou. 2010. Image Quality Metrics: PSNR vs. SSIM. In *2010 20th International Conference on Pattern Recognition*. 2366–2369. <https://doi.org/10.1109/ICPR.2010.579>
- [16] Weizhe Hua, Zhiru Zhang, and G. Edward Suh. 2018. Reverse Engineering Convolutional Neural Networks through Side-Channel Information Leaks. In *Proceedings of the 55th Annual Design Automation Conference*.
- [17] Gary B. Huang, Manu Ramesh, Tamara Berg, and Erik Learned-Miller. 2007. *Labeled Faces in the Wild: A Database for Studying Face Recognition in Unconstrained Environments*. Technical Report 07-49. University of Massachusetts, Amherst.
- [18] Phillip Isola, Jun-Yan Zhu, Tinghui Zhou, and Alexei A. Efros. 2017. Image-to-Image Translation with Conditional Adversarial Networks. *2017 IEEE Conference on Computer Vision and Pattern Recognition (CVPR)* (2017).
- [19] Matthew Jagielski, Nicholas Carlini, David Berthelot, Alex Kurakin, and Nicolas Papernot. 2020. High Accuracy and High Fidelity Extraction of Neural Networks. In *29th USENIX Security Symposium (USENIX Security 20)*.
- [20] Hengrui Jia, Christopher A. Choquette-Choo, Varun Chandrasekaran, and Nicolas Papernot. 2021. Entangled Watermarks as a Defense against Model Extraction. *arXiv:cs.CR/2002.12200*
- [21] Mika Juuti, Sebastian Szyller, Samuel Marchal, and N. Asokan. 2019. PRADA: Protecting against DNN Model Stealing Attacks. In *IEEE European Symposium on Security & Privacy*. IEEE, 1–16.
- [22] Sanjay Kariyappa and Moinuddin K Qureshi. 2019. Defending Against Model Stealing Attacks with Adaptive Misinformation. *arXiv:stat.ML/1911.07100*
- [23] T. Karras, S. Laine, and T. Aila. 2019. A Style-Based Generator Architecture for Generative Adversarial Networks. In *2019 IEEE/CVF Conference on Computer Vision and Pattern Recognition (CVPR)*.
- [24] Manish Kesarwani, Bhaskar Mukhoty, Vijay Arya, and Sameep Mehta. 2018. Model Extraction Warning in MLaaS Paradigm. In *34th Annual Computer Security Applications Conference*.
- [25] Junho Kim, Minjae Kim, Hyeonwoo Kang, and Kwang Hee Lee. 2020. U-GAT-IT: Unsupervised Generative Attentional Networks with Adaptive Layer-Instance Normalization for Image-to-Image Translation. In *International Conference on Learning Representations*.
- [26] Kalpesh Krishna, Gaurav Singh Tomar, Ankur Parikh, Nicolas Papernot, and Mohit Iyer. 2020. Thieves of Sesame Street: Model Extraction on BERT-based APIs.
- [27] Wei-Sheng Lai, Jia-Bin Huang, Narendra Ahuja, and Ming-Hsuan Yang. 2017. Deep Laplacian Pyramid Networks for Fast and Accurate Super-Resolution. In *IEEE Conference on Computer Vision and Pattern Recognition*.
- [28] C. Ledig, L. Theis, F. Huszar, J. Caballero, A. Cunningham, A. Acosta, A. Aitken, A. Tejani, J. Totz, Z. Wang, and W. Shi. 2017. Photo-Realistic Single Image Super-Resolution Using a Generative Adversarial Network. In *2017 IEEE Conference on Computer Vision and Pattern Recognition (CVPR)*.
- [29] Pengcheng Li, Jinfeng Yi, and Lijun Zhang. 2018. Query-Efficient Black-Box Attack by Active Learning. *arXiv preprint arXiv:1809.04913* (2018).
- [30] Ziwei Liu, Ping Luo, Xiaogang Wang, and Xiaoou Tang. 2015. Deep Learning Face Attributes in the Wild. In *Proceedings of International Conference on Computer Vision (ICCV)*.
- [31] Mario Lucic, Karol Kurach, Marcin Michalski, Olivier Bousquet, and Sylvain Gelly. 2018. Are GANs Created Equal? A Large-Scale Study. In *Proceedings of the 32nd International Conference on Neural Information Processing Systems*.
- [32] Datasets of pictures of natural landscapes. Accessed on April 12 2021. <https://kaggle.com/arnaud58/landscape-pictures>
- [33] Seong Joon Oh, Max Augustin, Mario Fritz, and Bernt Schiele. 2018. Towards Reverse-Engineering Black-Box Neural Networks. In *International Conference on Learning Representations*. <https://openreview.net/forum?id=BydJte0->
- [34] Tribhuvanesh Orekondy, Bernt Schiele, and Mario Fritz. 2019. Knockoff Nets: Stealing Functionality of Black-Box Models. In *CVPR*. 4954–4963.
- [35] Tribhuvanesh Orekondy, Bernt Schiele, and Mario Fritz. 2020. Prediction Poisoning: Towards Defenses Against DNN Model Stealing Attacks. *arXiv:cs.LG/1906.10908*
- [36] CycleGAN’s Monet Paintings and Natural Photos Dataset. Accessed on April 12 2021. <https://kaggle.com/balraj98/monet2photo>
- [37] Nicolas Papernot, Patrick McDaniel, Ian Goodfellow, Somesh Jha, Z Berkay Celik, and Ananthram Swami. 2017. Practical black-box attacks against machine learning. In *ACM Symposium on Information, Computer and Communications Security*. ACM, 506–519.
- [38] E. Quring, D. Arp, and K. Rieck. 2018. Forgotten Siblings: Unifying Attacks on Machine Learning and Digital Watermarking. In *IEEE European Symposium on Security & Privacy*. 488–502.
- [39] Evan Shelhamer, Jonathan Long, and Trevor Darrell. 2017. Fully Convolutional Networks for Semantic Segmentation. *IEEE Trans. Pattern Anal. Mach. Intell.* 39, 4 (2017), 640–651.
- [40] Sebastian Szyller, Buse Gul Atli, Samuel Marchal, and N. Asokan. 2020. DAWN: Dynamic Adversarial Watermarking of Neural Networks. *arXiv:cs.CR/1906.00830*
- [41] Tatsuya Takemura, Naoto Yanai, and Toru Fujiwara. 2020. Model Extraction Attacks against Recurrent Neural Networks. *arXiv:cs.CR/2002.00123*
- [42] TechWorld. 2018. How tech giants are investing in artificial intelligence. <https://www.techworld.com/picture-gallery/data/tech-giants-investing-in-artificial-intelligence-3629737>. Online; accessed 9 May 2019.
- [43] Ruben Tolosana, Ruben Vera-Rodriguez, Julian Fierrez, Aythami Morales, and Javier Ortega-Garcia. 2020. DeepFakes and Beyond: A Survey of Face Manipulation and Fake Detection.
- [44] Florian Tramèr, Fan Zhang, Ari Juels, Michael K Reiter, and Thomas Ristenpart. 2016. Stealing machine learning models via prediction apis. In *25th USENIX Security Symposium*. 601–618.
- [45] Eric Wallace, Mitchell Stern, and Dawn Song. 2021. Imitation Attacks and Defenses for Black-box Machine Translation Systems. *arXiv:cs.CL/2004.15015*
- [46] Mengjia Yan, Christopher W. Fletcher, and Josep Torrellas. 2020. Cache Telepathy: Leveraging Shared Resource Attacks to Learn DNN Architectures. In *29th USENIX Security Symposium (USENIX Security 20)*.
- [47] Ning Yu, Vladislav Skripniuk, Sahar Abdelnabi, and Mario Fritz. 2020. Artificial GAN Fingerprints: Rooting Deepfake Attribution in Training Data. *arXiv:cs.CR/2007.08457*
- [48] Jie Zhang, Dongdong Chen, Jing Liao, Han Fang, Weiming Zhang, Wenbo Zhou, Hao Cui, and Nenghai Yu. 2020. Model Watermarking for Image Processing Networks. *arXiv:cs.MM/2002.11088*
- [49] Huadi Zheng, Qingqing Ye, Haibo Hu, Chengfang Fang, and Jie Shi. 2019. BDPL: A Boundary Differentially Private Layer Against Machine Learning Model Extraction Attacks. In *Computer Security – ESORICS 2019*, Kazuo Sako, Steve Schneider, and Peter Y. A. Ryan (Eds.). Springer International Publishing, Cham, 66–83.
- [50] Zhou Wang, A. C. Bovik, H. R. Sheikh, and E. P. Simoncelli. 2004. Image quality assessment: from error visibility to structural similarity. *IEEE Transactions on Image Processing* 13, 4 (2004), 600–612. <https://doi.org/10.1109/TIP.2003.819861>
- [51] Jun-Yan Zhu, Taesung Park, Phillip Isola, and Alexei A Efros. 2017. Unpaired Image-to-Image Translation using Cycle-Consistent Adversarial Networks. In *Computer Vision (ICCV), 2017 IEEE International Conference on*.